

VUV/XUV measurements of impurity emission in plasmas with liquid lithium surfaces on LTX

This content has been downloaded from IOPscience. Please scroll down to see the full text.

2014 Plasma Phys. Control. Fusion 56 125014

(<http://iopscience.iop.org/0741-3335/56/12/125014>)

View [the table of contents for this issue](#), or go to the [journal homepage](#) for more

Download details:

IP Address: 198.125.230.204

This content was downloaded on 02/02/2015 at 23:13

Please note that [terms and conditions apply](#).

VUV/XUV measurements of impurity emission in plasmas with liquid lithium surfaces on LTX

Kevin Tritz¹, Ronald E Bell², Peter Beiersdorfer³, Dennis Boyle², Joel Clementson³, Michael Finkenthal¹, Robert Kaita², Tom Kozub², Shigeyuki Kubota⁴, Matthew Lucia², Richard Majeski², Enrique Merino², John Schmitt² and Dan Stutman¹

¹ Department of Physics, Johns Hopkins University, 3400 North Charles St., Baltimore, MD 21218, USA

² Princeton Plasma Physics Laboratory, 100 Stellarator Rd, Princeton, NJ 08543, USA

³ Lawrence Livermore National Laboratory, 7000 East Ave., Livermore, CA 94550, USA

⁴ Department of Physics and Astronomy, UCLA, 475 Portola Plaza, Los Angeles, CA 90095, USA

E-mail: ktritz@pppl.gov

Received 2 July 2014, revised 13 October 2014

Accepted for publication 23 October 2014

Published 12 November 2014

Abstract

The VUV/XUV spectrum has been measured on the Lithium Tokamak eXperiment (LTX) using a transmission grating imaging spectrometer (TGIS) coupled to a direct-detection x-ray charge-coupled device camera. TGIS data show significant changes in the ratios between the lithium and oxygen impurity line emission during discharges with varying lithium wall conditions. Lithium coatings that have been passivated by lengthy exposure to significant levels of impurities contribute to a large O/Li ratio measured during LTX plasma discharges. Furthermore, previous results have indicated that a passivated lithium film on the plasma facing components will function as a stronger impurity source when in the form of a hot liquid layer compared to a solid lithium layer. However, recent TGIS measurements of plasma discharges in LTX with hot stainless steel boundary shells and a fresh liquid lithium coating show lower O/Li impurity line ratios when compared to discharges with a solid lithium film on cool shells. These new measurements help elucidate the somewhat contradictory results of the effects of solid and liquid lithium on plasma confinement observed in previous experiments.

Keywords: XUV, lithium, tokamak, spectroscopy

(Some figures may appear in colour only in the online journal)

1. Introduction

One of the primary challenges to the successful implementation of fusion energy is the survivability of the vessel wall materials exposed to the plasma particle and heat exhaust. The extremely high heat loads combined with large energetic particle fluxes can cause erosion of exposed surfaces, especially in the plasma divertor region, which will dramatically reduce component lifetime [1]. To mitigate these effects, the use of liquid metal first wall materials has been proposed as a solution to solid surface material remodeling and erosion in the high particle and heat flux environment of tokamak divertors.

The advanced limiter-divertor plasma-facing systems (ALPS) program was created to evaluate the characteristics of liquid metal surfaces across a variety of experimental devices to demonstrate the advantages of an advanced limiter system in handling large peak heat flux $>50\text{ MW m}^{-2}$, lifetime erosion limits, and efficient heat extraction [2]. While studies have identified tin, gallium, and lithium as potential candidates for advanced divertor liquid metal surfaces, to date the ALPS program has evaluated the deployment of lithium on fusion research devices [3].

The primary mission of the Lithium Tokamak eXperiment (LTX) is to investigate the effects of a lithium boundary and

associated low particle recycling, on plasma confinement and performance [4]. The machine is designed with a set of stainless steel metal shell liners bonded to copper shells which provide a close-fitting boundary to the plasma with nearly complete poloidal and toroidal coverage. Lithium is evaporated onto the shells using either an electron beam (e-beam) to heat a lithium pool in the bottom of the machine or evaporated from an inserted, heated crucible. In addition, heating coils on the metal shells can raise their surface temperature above the lithium melting point, which allows a comparison between the effects of solid and liquid lithium as a plasma facing component (PFC).

Both the LTX machine and its mission are expansions of the previous work on the Current Drive eXperiment Upgrade (CDX-U) which demonstrated a substantial confinement improvement when the plasma discharge utilized a liquid lithium limiter boundary [5]. In that case, the factor of ~5–10 confinement improvement was obtained with only partial PFC coverage by a liquid lithium pool in a tray at the bottom of the vessel. While comprehensive measurements of the plasma conditions were limited by diagnostic availability, a low recycling transport model was able to reproduce the features of the CDX-U observations [4, 6]. These results motivated the design and construction of LTX, as well as the initiation of the liquid lithium divertor (LLD) program on the National Spherical Tokamak Experiment (NSTX) [7].

2. Previous LTX experimental results

Previous experiments on LTX have investigated the effects of solid and liquid lithium films on plasma performance [8]. Plasma discharges with bare stainless steel as the first wall severely limit the machine performance, with a maximum plasma current of ~10 kA and a sustained duration of less than 5 ms. However, with a thin solid lithium film coating the stainless surfaces LTX routinely achieves plasma currents of ~65 kA and can achieve pulse lengths exceeding 30–40 ms. The lithium deposition procedure for these previous experiments is described in detail in [5], and consisted of evaporating lithium from a heated crucible into the vessel with a backfill of 1–5 mTorr of helium gas. Over the course of days, the lithium would gradually saturate by absorbing and reacting with hydrogen and impurity atoms. Thus, the surface no longer provided a low-recycling, clean wall, and as a result it became a net particle source for the plasma. At this point fresh lithium would be evaporated onto the shells, thus burying the previously passivated surface layer and restoring the low-recycling character of the lithium PFC.

The first results from the experiments testing hot shells with a liquid lithium surface showed much lower performance, overall, than the solid lithium, room-temperature shell discharges. Measurements of injected particle inventories indicated that liquid lithium had a lower pumping capacity than the solid lithium film, and would even act as a net particle source in some discharges. Furthermore, data from the residual gas analyzer (RGA) showed higher

background levels of water and other trace impurity gases during hot wall operation. As a result, the plasma discharge length was shortened to <20 ms with the plasma current limited to <10 kA. Subsequent experiments scanned the shell temperature and found a sharp decrease in plasma performance once the PFC temperature exceeded the melting point of lithium. However, base vacuum conditions had improved such that the impurity levels reflected in the RGA spectrum were essentially identical across the range of lithium temperature. This would appear to eliminate background vacuum conditions as the cause of the degraded performance.

Furthermore, spectroscopic measurements suggested that the liquid lithium layer acted as a significant impurity particle source. A single channel extreme ultraviolet (EUV) spectrometer provided by Lawrence Livermore National Laboratory covered a large enough spectral range to monitor the Li and O impurity emission [9]. During the higher performance, solid wall discharges, the EUV spectrometer measured line emission from Li III as well significant emission from higher charge states of oxygen, O V and O VI. However, the electron temperatures of the reduced performance discharges with the hot shells and liquid lithium film were far too low to excite these spectral lines. Instead, a visible spectrometer measuring the lower O II charge state showed a dramatic increase in emission during liquid lithium discharges by roughly an order of magnitude. Similarly, normalized D- α measurements associated with neutral particle density increased by a factor of ~3 [8].

The general conclusion of these experiments was that a solid lithium film was more effective at pumping and retaining the hydrogen particles as well as absorbing and sequestering impurity atoms. Liquid films allowed a significant interaction between the plasma and the dissolved impurity species, acting as both a net hydrogen source as well as a substantial source of impurity particles. One caveat mentioned in the previous work was that these experiments were performed after a long experimental campaign, covering over a year of operation under variable vacuum conditions with intermittent leaks and periodic lithium evaporations. As such, a significant amount of oxygen and other impurities was sequestered in the machines total internal lithium inventory of LTX. Therefore, even after a fresh coating of lithium was evaporated onto the shells, it is reasonable to propose that once the lithium melted, the large inventory of dissolved impurities could have mobilized and reached the surface of the film, ready to interact with the plasma boundary.

Recent experiments sought to remedy these aforementioned complications by evaporating fresh lithium into a clean machine with improved vacuum conditions. Furthermore, the evaporation procedure was altered to utilize an e-beam heating system, similar to what was used for the CDX-U experiments, which provided a shorter passivation time between the evaporative deposition on the shells and the plasma discharge. Results from these new experiments will be discussed in section 4. Finally, improved diagnostic coverage helped elucidate the plasma response to the different lithium wall conditions.

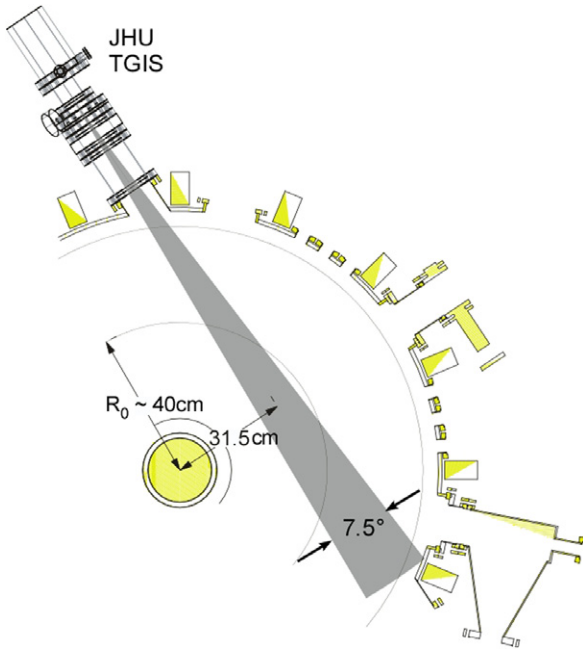


Figure 1. Top down view of the LTX vacuum vessel midplane illustrating the intersection of the TGIS field of view with the canonical plasma major radius.

3. Diagnostics and measurement technique

The transmission grating imaging spectrometer (TGIS), designed and built by the Johns Hopkins University spectroscopy group is a compact and highly portable instrument which provides a spatially resolved XUV/VUV spectrum from $\sim 50\text{--}700\text{\AA}$ with time resolution $<20\text{ms}$ [10]. Previous versions of the TGIS have been used on NSTX to provide spatially resolved monitoring of impurities during a variety of discharges with lithium-coated and lithium-free PFCs [11]. The diagnostic system has since been upgraded with a PIXIS-400B direct detection x-ray CCD from Princeton Instruments [12] to improve the sensitivity and stability of the measurement, with the ultimate goal of absolute and spectrally resolved radiated power measurements of the tokamak core, edge, and divertor region [13, 14].

At present, the TGIS is installed on the LTX midplane, with a spatial view oriented tangentially across the plasma core (figure 1). As shown in the diagnostic layout, the restricted field of view of the present TGIS limits the ability to extract spatial information from the LTX discharges. Direct inversions of the data are not feasible without a field of view that encompasses the outer plasma edge. Furthermore, the limited diagnostic set currently available on LTX prevents the use of equilibrium flux-surface based modeling of the impurity spectra for a forward modeling fitting calculation of the impurity local emissivities [15]. Therefore, the present analysis forgoes the spatial information contained in the TGIS measurement, and bins the individual spatial channels together to improve the photon statistics and signal to noise ratio of the measured impurity lines.

Figure 2 shows the TGIS data from an LTX discharge. The image in figure 2(a) displays impurity line emission

with the spectral range aligned with the x -axis, and the spatial dimension arranged vertically. The image data has been smoothed and ‘despiked’ to remove incident x-ray detection events, which can significantly pollute the underlying VUV/XUV spectrum. This filtering process involves fitting a smoothing spline across the spatial extent of each spectral column to characterize the underlying plasma emission at each wavelength while excluding the noisy ‘spikes’ from each x-ray [16]. This smoothing method is preferable to a general 2D median filter as it preserves the spectral resolution of the diagnostic. Next, the spatial data in each spectral column is binned, resulting in the plot shown in figure 2(b) after the wavelength calibration has been applied. The plotted spectrum shows clear emission lines from Li III and higher charge states of oxygen, O V and O VI. The spectral resolution is limited by the instrumental function to $\sim 10\text{\AA}$, thereby blending the various groups of oxygen charge state line emission. The corresponding spectral lines of the primary charge state emissions are listed in table 1 [17].

The next stage of the analysis involves fitting Gaussian functions to each envelope of line emission (figure 3). While the instrumental width of the TGIS is too large to measure ion temperatures via spectral line broadening, the amplitude of the fitted Gaussian curves will provide a measure of the relative influx and concentration of lithium and oxygen impurities in the plasma. However, one cannot simply compare either absolute or even relative magnitudes of each spectral line between two discharges for several reasons. The total emission power of each Li and O spectral line, calculated by the CHIANTI coronal atomic spectral model [18, 19], is a strong function of electron temperature, decreasing by an order of magnitude in the estimated range of the LTX discharges with $T_{e0} \sim 50\text{--}100\text{eV}$. Furthermore, the modest electron density, $n_{e0} \sim 0.5\text{--}0.8 \times 10^{19}\text{m}^{-3}$, combined with the relatively short particle confinement times, $\tau_p \sim \tau_E \sim 2\text{--}7\text{ms}$, provides a product $n_e\tau_p$ of $\sim 1\text{--}5 \times 10^{16}\text{m}^{-3}\text{s}$, which is roughly 1–2 orders of magnitude below the value required for local thermodynamic equilibrium. Thus, simple coronal atomic spectral models are insufficient to accurately relate the impurity line emission to impurity concentration, even with precise measurements of the electron temperature and density. Furthermore, full impurity transport code analysis requires more complete diagnostic information than is presently available for this work.

A solution to this dilemma takes advantage of the fact that the ionization energies of the dominant emitting charge states: Li III (113 eV), O V (110 eV), and O VI (138 eV) are not too dissimilar. Therefore, using the ratios of the oxygen charge state emission lines to the primary Li III line at 135\AA can largely eliminate this complex dependence on T_e and $n_e\tau_p$. In fact, comparing the ensemble averaged radiated power for oxygen [20] and lithium [21] at the estimated values of $n_e\tau_p$, one finds that both elements have a similar radiative power decrease of $\sim 50\%$ over the temperature range of interest; thus, comparing the values of the O/Li line ratios from each shot will isolate the effects of changes in the impurity particle source.

Finally, a remaining issue is one of measurement ‘localization’ in both time and space. The TGIS instrument exposes

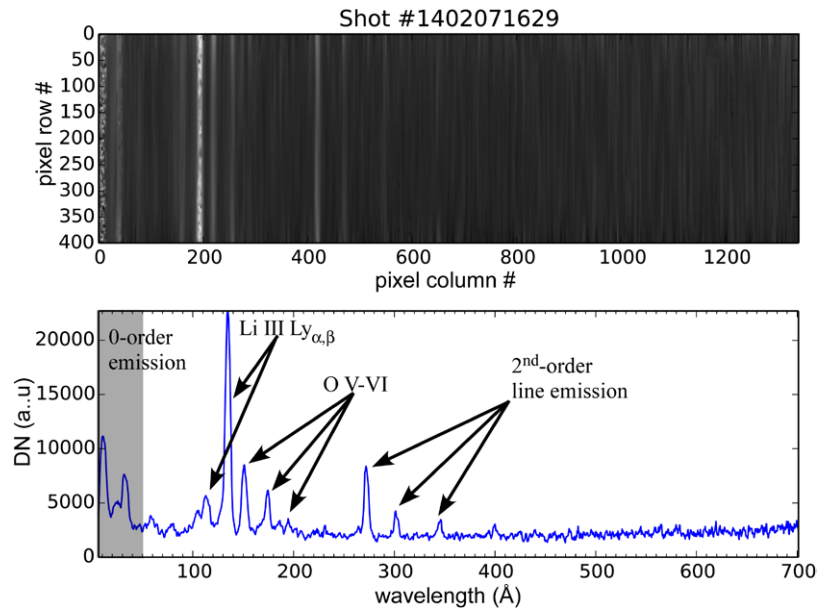


Figure 2. (a) Smoothed image from TGIS PIXIS-400B CCD camera and (b) wavelength-adjusted spectrum with full spatial binning showing line emission from multiple charge states of O and Li (see figure 3, table 1 for details).

Table 1. List of charge states for dominant impurity line emission with corresponding wavelengths and atomic level transitions for LTX discharges.

Ion	Wavelength (Å)	Level transitions
Li III	113.9	$1s \rightarrow 3p$
Li III	135.0	$1s \rightarrow 2p$
O VI	150.1	$1s^2 2s \rightarrow 1s^2 3p$
O V	172.2	$1s^2 2s^2 \rightarrow 1s^2 2s 3p$
O VI	172.9–173.1	$1s^2 2p \rightarrow 1s^2 3d$
O VI	183.9–184.1	$1s^2 2p \rightarrow 1s^2 3s$
O V	192.7–192.9	$1s^2 2s 2p \rightarrow 1s^2 2s 3d$

the CCD chip for 40 ms, integrating over the entire plasma discharge of ~ 30 ms. Additionally, the line integrated nature of radiation detection combined with the restricted field of view on LTX hinders precise spatial localization, as discussed previously. How localized, then, are the measured emission lines? To address this question, data for the impurities measured by the TGIS were obtained with a high resolution visible light spectrometer (HAL) to provide improved spatial and temporal resolution of 1–2 cm, and 2.5 ms respectively [22]. The visible spectrometer, which can be scanned from 400 to 820 nm was centered on a visible line of Li III at 451 nm, with data from the spectrometer shown in figure 4 for shot 1402071629. The multiple spatial chords of the spectrometer permit an inversion of the line-integrated brightness to obtain localized emissivity. Correspondingly, the data in figure 4(b) show a peaking of the Li III emission near the estimated center of the plasma. Furthermore, the time history of the Li III emission shown in figure 4(a) confirms that the majority of the measured Li III radiation occurs within a ~ 10 ms ‘hot’ phase of the plasma discharge, during which time the plasma reaches and sustains its peak net current. The HAL spectral data show little to no Li III emission during the plasma breakdown and current ramp

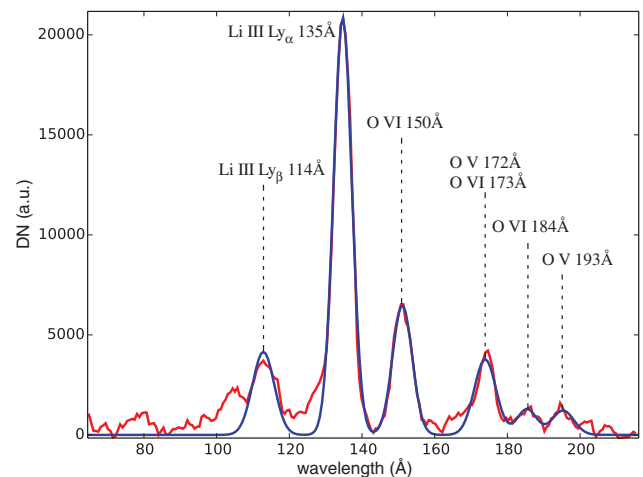


Figure 3. Close up view of the spectral range of interest showing fitted Gaussian signals to the Li III, O V, and O VI emission lines.

or from the atomic recombination phase during the plasma quench. While the HAL spectrometer was unable to view O V, or O VI visible line emission, the similarity in the response to temperature and particle confinement mentioned previously lends confidence that the higher charge state oxygen emission measured by the TGIS is likewise confined to the plasma core during the ~ 10 ms of peak electron temperature. Therefore, even with the spatial and temporal resolution limitations of the TGIS on LTX, incorporation of the information from the HAL spectrometer allows a temporal and spatial localization of the XUV impurity line emission.

4. Experimental results

This analysis of recent experiments on LTX characterizes the effects of lithium coatings by comparing three distinct

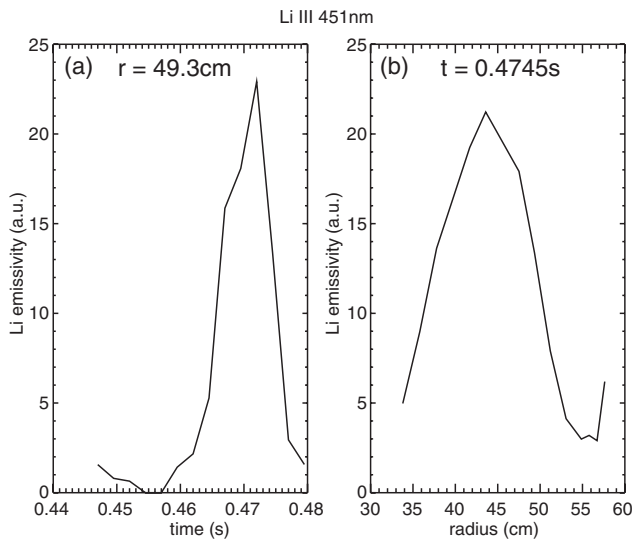


Figure 4. Li III visible emissivity measured by the HAL spectrometer showing (a) time history and (b) radial localization of the impurity line emission at 450 nm.

scenarios. The TGIS spectra of representative discharges for each scenario are shown in figure 5. It should be noted that the varying baseline of the spectra corresponds to un-subtracted dark current, and all line emission measurements and ratios are taken with this baseline subtracted. The wall conditions for the first set of discharges consist of a room-temperature shell with a fresh solid lithium layer, evaporated 1 day earlier with a total deposition of 82 ± 28 mg, over a solid layer of older lithium depositions. The fresh lithium surface had been semi-passivated through exposure to trace impurities at a base pressure near the mid 10^{-8} Torr range, as well as ~ 30 plasma discharges. Figure 5(a) shows the TGIS spectrum for a discharge near the end of this run, which displays several important characteristics. The higher O V/O VI line ratio and significant presence of line emission at 193 \AA indicates a core electron temperature closer to $40\text{--}50 \text{ eV}$, much lower than the $\sim 100 \text{ eV}$ estimates for the discharges with fresh lithium. Additionally, the O VI/Li III line ratios are quite high (i.e. ~ 1), which suggests a strongly enhanced oxygen impurity source relative to the lithium. Finally, the absolute magnitude of the Li III line emission is $\sim 50\%$ higher than the ‘fresh’ solid lithium PFC experimental run, after normalizing for the line-averaged density variations. This increase in radiated power is consistent with an overall lower electron temperature for the semi-passivated discharges, as indicated by the enhanced O V emission.

The subsequent experimental run was initiated following a period of e-beam heating of the bottom lithium pool and evaporation onto the heated shells. A total of 197 ± 75 mg was evaporated onto the shell surfaces with two out of the four shells maintained at 300°C . Shortly after the end of the e-beam evaporation, a typical plasma discharge was established and run throughout the day, with a representative TGIS spectrum shown in figure 5(b). This spectrum shows clear differences from the discharges on the semi-passivated lithium. The O/Li line ratios have decreased by an order of magnitude. Additionally, the amplitude of the lithium line is lower by

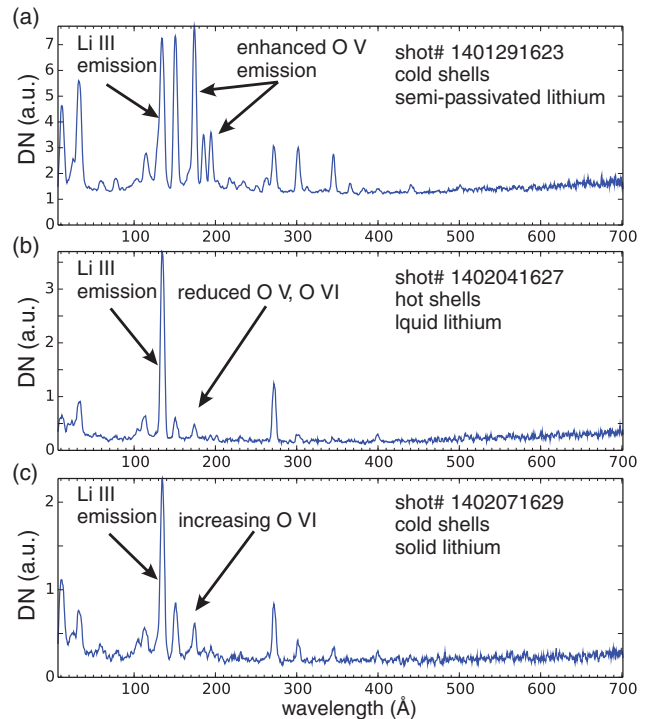


Figure 5. Representative TGIS spectra from three different PFC experimental scenarios: (a) solid, semi-passivated lithium film, (b) freshly-evaporated liquid lithium film, and (c) refreshed solid lithium film.

$\sim 40\%$, which, given a similar line averaged electron density, indicates a higher core electron temperature, $\sim 100 \text{ eV}$, further supported by the significant reduction of O V line radiation relative to O VI.

For the final set of discharges three days later, no new lithium was evaporated and all shells were maintained at room temperature providing a fully solid lithium first wall surface material to the plasma. The plasma bulk parameters of the discharges (e.g. plasma current, density, pulse length) were generally comparable to the previous campaign with the liquid lithium surfaces. However, the TGIS spectra for these plasmas (figure 5(c)) show important differences. While overall, the spectra were similar to the liquid lithium case (5(b)), the O/Li line ratios were $\sim 3\text{--}6$ times higher, indicating a comparably higher oxygen impurity concentration and source rate from the lithium PFCs.

By plotting the O/Li ratios for each discharge over the course of the experimental run days, one obtains a comprehensive picture of the differences in the measured TGIS spectral emission between the solid and liquid lithium scenarios (figure 6(a)). It is clear from the data that the ratios are significantly and consistently higher with solid lithium films compared to the discharges with liquid lithium PFCs. Additionally, even considering the shot-to-shot variability, there is an upward trend in the measured ratios throughout the day, indicating a gradual reduction of the pumping and sequestration efficacy of the solid lithium surface.

However, the discharges with the liquid lithium surfaces show a very different trend. Not only is there a much lower shot-to-shot variability in the measured line emission ratios,

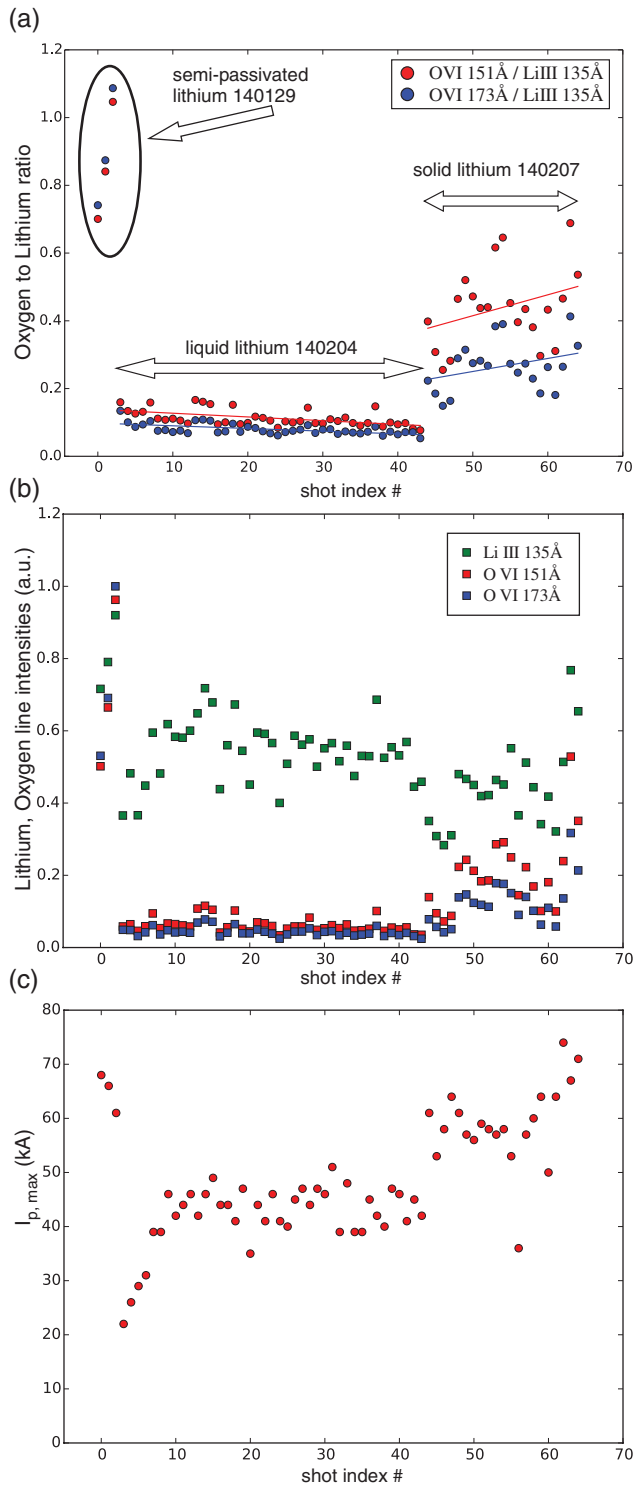


Figure 6. (a) O VI/Li III line ratios as a function of shot index for the solid, semi-passivated lithium, fresh liquid lithium, and refreshed solid lithium experimental campaigns with (b) corresponding Li and O impurity line intensities, and (c) maximum plasma current for each shot.

but the overall trend is flat to slightly declining over dozens of plasma shots. This trend indicates that liquid lithium films have a large capacity to absorb and sequester impurities, while maintaining a clean first wall. Another potential factor was the continuous, low-level lithium evaporation from the hot shells

during the experimental run, which accounted for ~10 mg out of the ~200 mg deposition.

For completeness, the individual impurity line intensities used in the ratio calculation are shown in figure 6(b). The lower ratios in the liquid lithium discharges are clearly attributable to the much lower intensity of the oxygen line emission. This is consistent with a significantly reduced inventory of oxygen ions in the main plasma. Conversely, the lithium intensity is less differentiated between the three scenarios, with only a modest average increase during the liquid lithium discharges. Finally, figure 6(c) shows the maximum plasma current obtained during each discharge for the different lithium scenarios. While the solid surface discharges have typical plasma currents in the ~50–70 kA range, the hot-shell liquid lithium discharges generally achieve ~40–50 kA. This result is in contrast to previous results from [5]—figure 8, which showed a significant decrease in maximum plasma current from ~30 to <10 kA when the LTX shells were heated above the Li melting temperature.

In those previous discharges, the large influx of H₂ gas and impurities from a saturated liquid lithium substrate severely degraded the plasma performance. However, in the present results, the modest reduction in plasma current is primarily attributed to difficulties in optimizing the gas fueling and coil waveforms to the hot-shell scenario. Given the lack of plasma feedback control, the gas fueling and coil waveforms are all pre-programmed with an ‘open-loop’ control system. In the hot-shell scenario, the change in resistivity of the boundary shells from the elevated temperatures, along with the large increase in pumping rate of the lithium substrate require significant changes to the LTX control waveforms. Further optimizations in subsequent experiments have since improved the maximum plasma current in hot-shell scenarios to ~60 kA.

5. Discussion

As mentioned previously, results of comparisons between solid and liquid lithium surfaces have varied significantly on different devices, and under different experimental conditions. In fact, the present positive liquid lithium results, and the previous LTX results showing extremely poor plasma response to a liquid lithium surface may have a common explanation: the mobility of impurities in a liquid lithium substrate.

With a solid lithium surface, any bonding of an impurity to the surface leaves that impurity exposed and available for plasma surface interactions. Furthermore, as coverage of the reacted lithium surface grows, its pumping and impurity sequestration efficacy will decline, as shown by the increasing O/Li ratio in the above data, as well as through extensive operational experience on LTX, CDX-U, and NSTX. Thus, solid lithium surfaces are routinely refreshed by periodic evaporations, which effectively bury the passivated surface and maintain sequestration of the reacted impurities.

However, as demonstrated by the previous LTX results, a lithium substrate that is heavily saturated with impurities can readily release these impurities when melted, causing a significant impurity influx into the plasma. The increased mobility of

the impurity atoms in the liquid substrate suggests that the entire lithium *volume* within some depth determined by the dissolved atomic mobility is ultimately available for plasma–surface interactions. If this volume has a high concentration of impurities, then it can act as a large net source. Conversely, if the liquid lithium film is relatively pristine, as was the case in the present LTX study, then that specific volume is available to pump and sequester the impurities in the plasma edge. Thus, instead of a slowly degrading solid lithium pumping surface, the liquid lithium film offers much higher storage capacity and more longevity for hydrogen pumping and impurity sequestration.

Though the present results show that the liquid lithium film has a significant advantage over the solid lithium surface when it comes to impurity sequestration, the experience of the previous LTX results highlights an important caveat. It is straightforward to refresh a solid lithium film that has been passivated by merely evaporating a fresh layer to bury the impurities. However, to maintain an effective liquid PFC, it would have to be replaced with clean liquid because of its capacity to retain impurities throughout its bulk. In the context of next generation, long-pulse machines, this suggests a flowing liquid lithium system.

In conclusion, the enhanced pumping and sequestration of liquid lithium reported in this work suggests a plausible mechanism to explain the variations in pumping efficacy comparisons between solid and liquid lithium observed on both LTX and NSTX. To optimize the impact of liquid lithium on plasma pumping and recycling, it is essential to maintain good vacuum conditions to reduce the accumulation of dissolved impurities, as well as periodically refresh any thin PFC films from a reservoir of clean lithium. Merely burying a heavily passivated film by a thin layer of evaporated lithium is insufficient to maintain impurity sequestration for a melted lithium first wall material. This prescription can be used to guide future experimental campaigns with the goal of evaluating liquid lithium as a viable PFC for next-step fusion devices.

Acknowledgments

This work is supported by the Department of Energy grant numbers: DE-FG02-09ER55012, and at LTX by the DoE contract numbers: DE-AC02-09CH11466 and DE-AC05-00OR22725.

References

- [1] van der Laan J G, Akiba M, Hassanein A, Seki M and Tanchuk V 1991 *Fusion Eng. Des.* **18** 135
- [2] Mattas R F *et al* 2000 *Fusion Eng. Des.* **49–50** 127
- [3] Brooks J N *et al* 2005 *Fusion Sci. Technol.* **47** 669
- [4] Majeski R *et al* 2009 *Nucl. Fusion* **49** 055014
- [5] Kaita R, Majeski R, Gray T, Kugel H, Mansfield D, Spaleta J, Timberlake J and Zakharov L 2007 *Phys. Plasmas* **14** 056111
- [6] Majeski R, Doerner R, Gray T, Kaita R, Maingi R, Mansfield D, Spaleta J, Soukhanavskii V, Timberlake J and Zakharov L 2006 *Phys. Rev. Lett.* **97** 075002
- [7] Maingi R *et al* 2011 *Phys. Rev. Lett.* **107** 145004
- [8] Majeski R *et al* 2013 *Phys. Plasmas* **20** 056103
- [9] Clementson J H T, Beiersdorfer P, Magee E W, Layne D A, Kaita R, Majeski R and Barnsley R 2012 *Proc. 19th Topical Conf. on High Temperature Plasma Diagnostics (Monterey, CA, 6–10 May 2012)*
- [10] Kumar D, Finkenthal M, Stutman D, Bell R E, Clayton D J, Diallo A, LeBlanc B P, Podesta M and Tritz K 2012 *Plasma Phys. Control. Fusion* **54** 065010
- [11] Kumar D, Stutman D, Tritz K, Finkenthal M, Tarrío C and Grantham S 2010 *Rev. Sci. Instrum.* **81** 10E507
- [12] www.princetoninstruments.com/Uploads/Princeton/Documents/Datasheets/Princeton_Instruments_PIXIS_XO_400B_rev_N2_9.6.2012.pdf
- [13] Clayton D J, Stutman D, Jaworski M A, Finkenthal M, Kumar D and Tritz K 2012 *Rev. Sci. Instrum.* **83** 10D521
- [14] Kumar D, Clayton D J, Parman M, Stutman D and Tritz K 2012 *Rev. Sci. Instrum.* **83** 10E511
- [15] Tritz K, Stutman D, Delgado-Aparicio L and Finkenthal M 2006 *Rev. Sci. Instrum.* **77** 10F510
- [16] Reinsch C H 1967 *Numer. Math.* **10** 177
- [17] Kramida A, Ralchenko Yu, Reader J and NIST ASD Team 2013 *NIST Atomic Spectra Database (version 5.1)* (<http://physics.nist.gov/asd>) National Institute of Standards and Technology, Gaithersburg, MD
- [18] Dere K P, Landi E, Mason H E, Monsignor Fossi B C and Young P R 1997 *Astron. Astrophys. Suppl. Ser.* **125** 149
- [19] Landi E, Young P R, Dere K P, Del Zanna G and Mason H E 2013 *Astrophys. J.* **763** 86
- [20] Carolan P G and Piotrowicz V A 1983 *Plasma Phys.* **25** 1065
- [21] Mirnov S V, Azizov E A, Evtikhin V A, Lazarev V B, Lyublinski I E, Vertkov A V and Prokhorov D Yu 2006 *Plasma Phys. Control. Fusion* **48** 821
- [22] Bell R E 2014 *Rev. Sci. Instrum.* **85** 11E404 <http://dx.doi.org/10.1063/1.4884612>